Figure 9.54 Nodule sizes and types from photo-profiles and box-cores

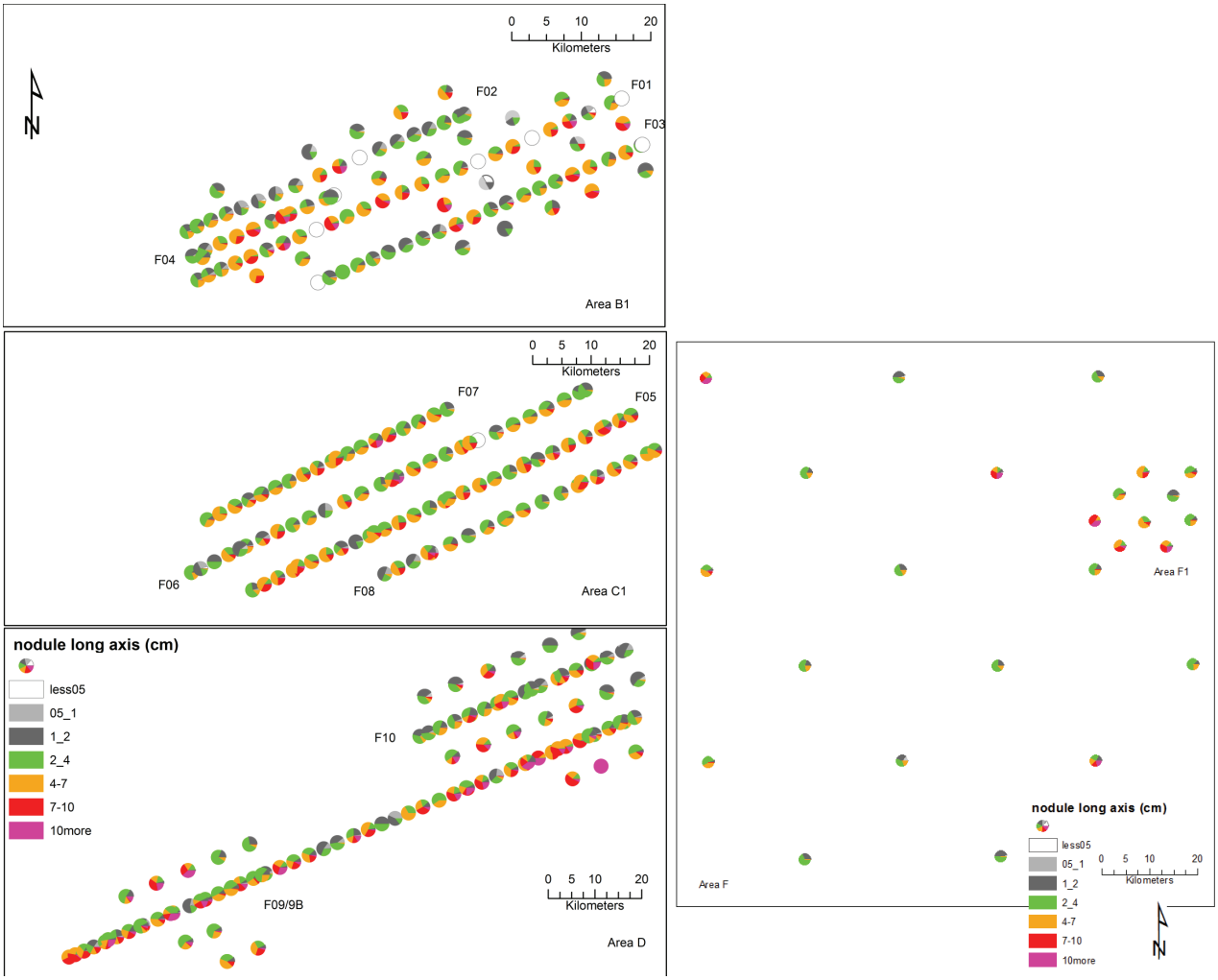

Top: B1, Middle-left: C1, Bottom-left: D1-D2, Bottom right: F and F1

All the surveyed areas host nodules of different sizes but Area B has mixed sized nodules and includes many of the smaller nodules. In Area C, nodule size increases to an average of small to medium and they are well distributed throughout. Within Area D, there is a mixture of sizes with some very large nodules found in the box-core samples. Bigger nodules were recovered from the box-corer than measured on the photo-profiling lines due to a frequent underestimation related to the sediment cover in this area. Area F has typically medium sized nodules but very large size nodules are seen in places.

Photos were also logged as they were collected for visible megafauna with preliminary logging results in Figure 9.55.

Figure 9.55 Neptune Photo-profile preliminary logging summary distribution of megafauna

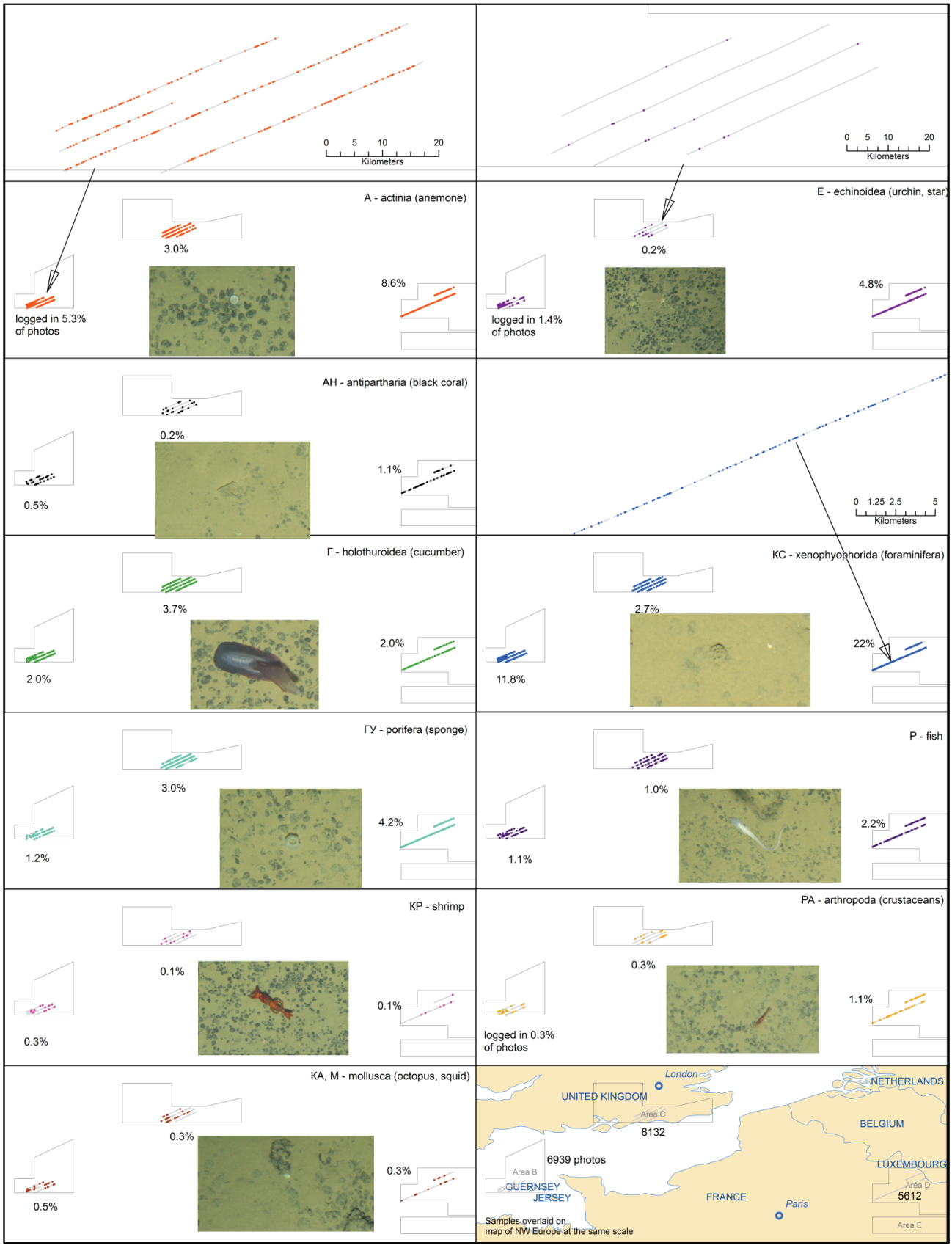

Some examples of the main types of megafauna seen in the photo-profiling conducted by TOML during the CCZ15 cruise are shown below. The photos were selected effectively at random from logging codes of the ~20,000 photos captured during that cruise.

Figure 9.56 Two genus Actinia (sea anemone) in Area C1

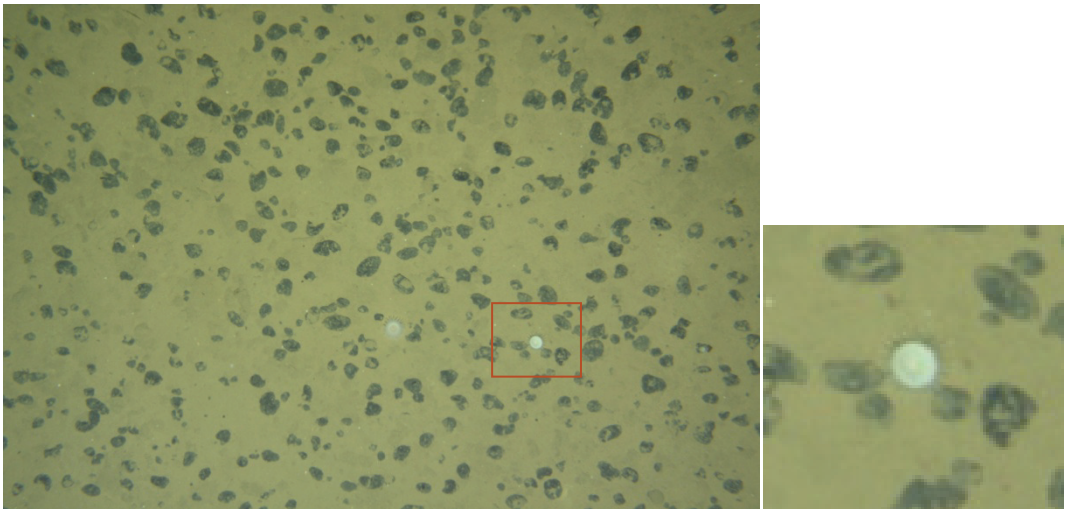

Main photo: 2.4 x 1.5 m; CCZ15-F08: 2015_09_08_154911

Figure 9.57 Order Antipatharia (black coral) in Area B1

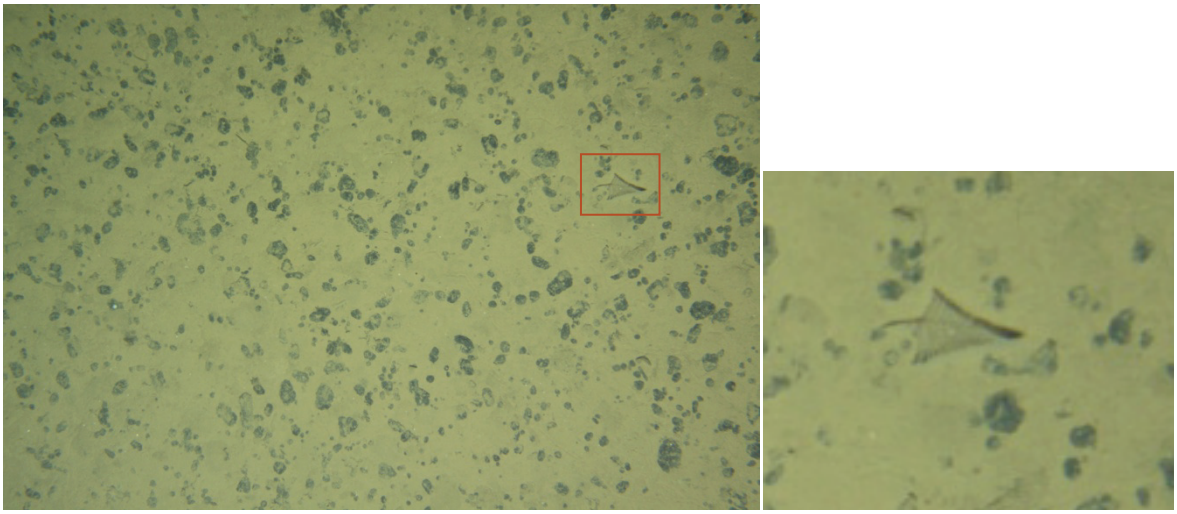

Main photo: 2.4 x 1.5 m; CCZ15-F03: 2015_08_21_205254

Figure 9.58 Class Holothuroidea (sea cucumber) in Area D

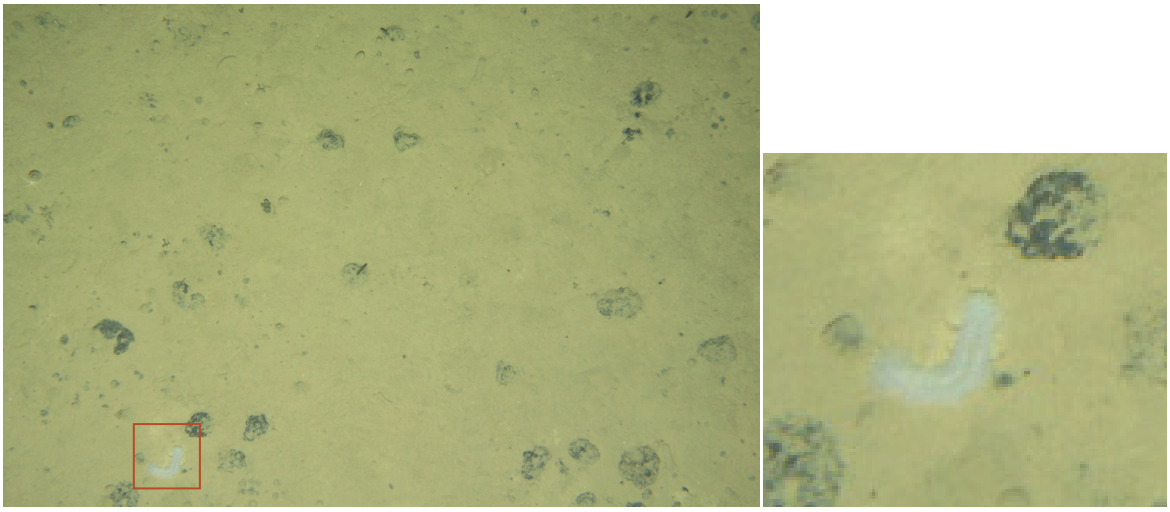

Main photo: 2.4 x 1.5 m; CCZ15-F09B: 2015_09_14_185421

Figure 9.59 Phylum Porifera (sponge) in Area B1

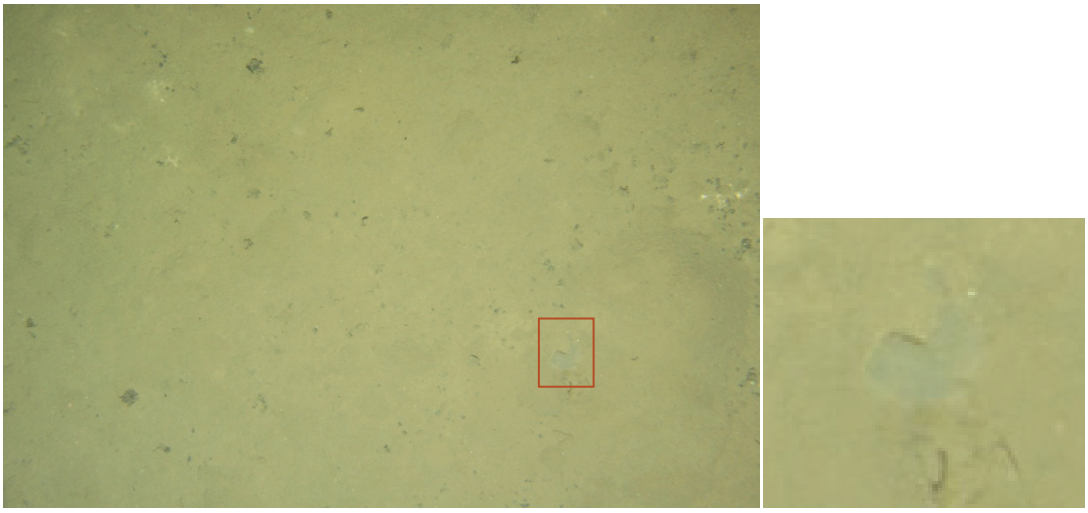

Main photo: 2.4 x 1.5 m; CCZ15-F04: 2015_08_26_082625

Figure 9.60 Class Echinoidea (sea urchin) in Area D2

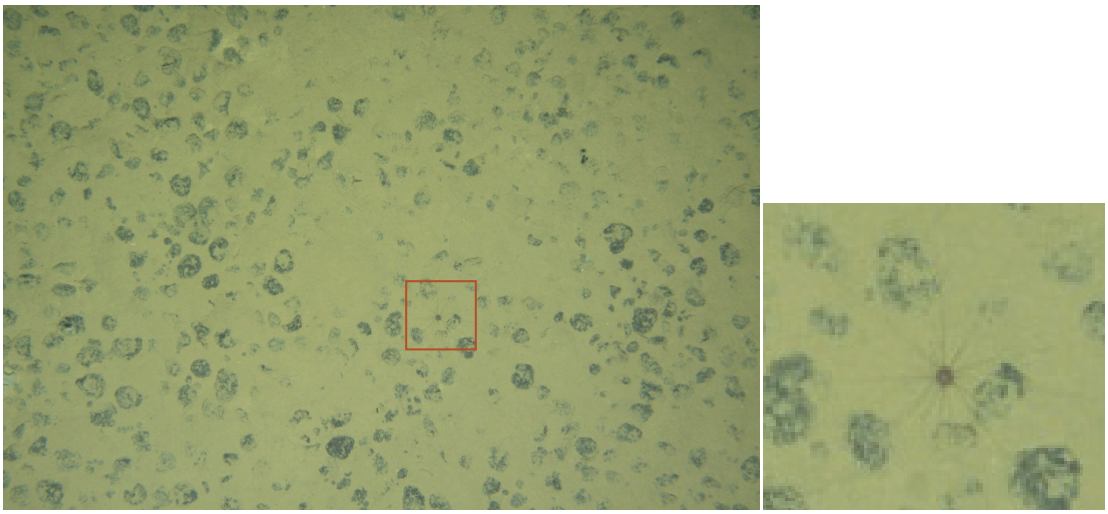

Main photo: 2.4 x 1.5 m; F10: 2015_09_16_070625

Figure 9.61 Order Decapoda (shrimp) in Area C1

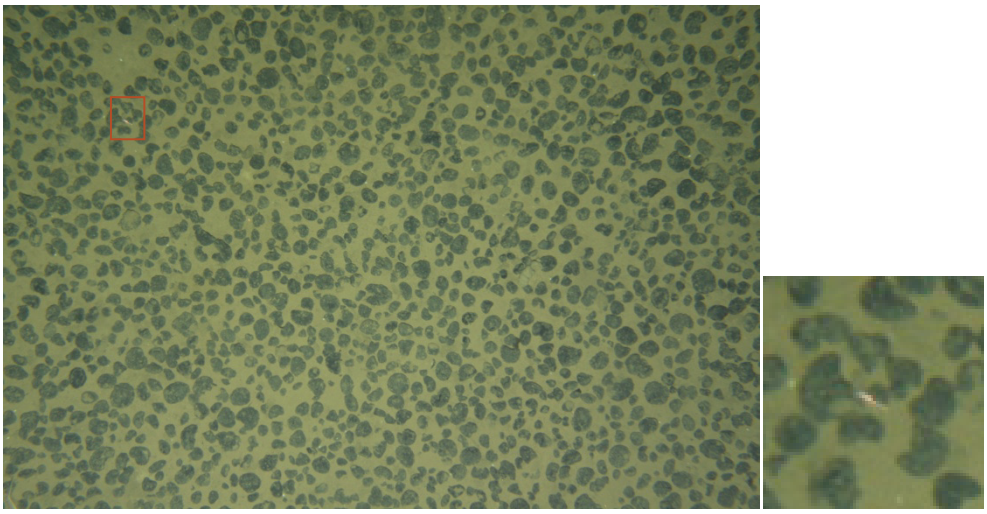

Main photo: 2.4 x 1.5 m; CCZ15-F05: 2015_08_29_060636

Figure 9.62 Order Teuthida (squid) in Area B1

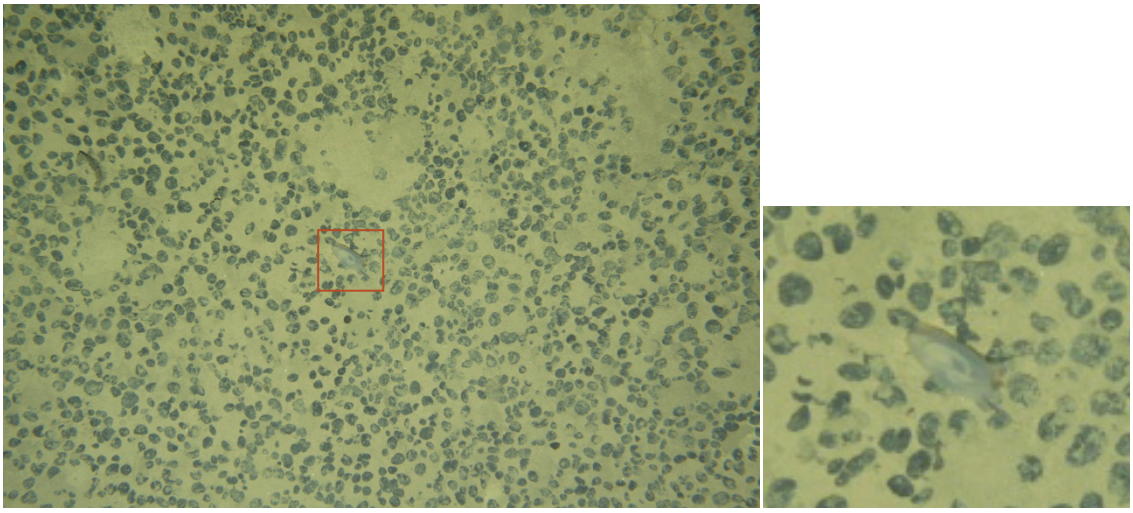

Main photo: 2.4 x 1.5 m; CCZ15-F01: 2015_08_11_110540

Figure 9.63 Fish in Area C

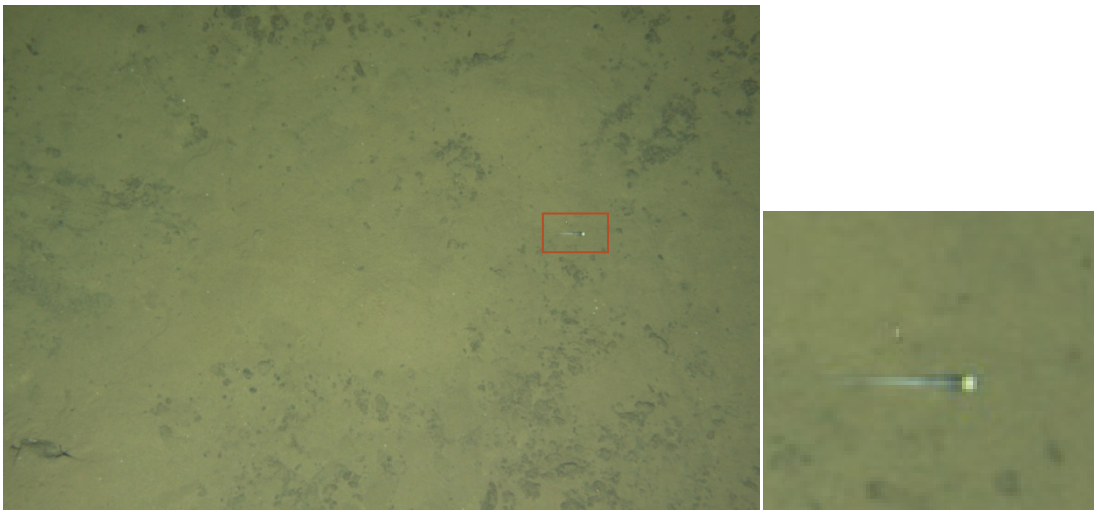

Main photo: 2.4 x 1.5 m; CCZ15-F06: 2015_09_02_190522

Figure 9.64 Phylum Arthropoda (excludes decapods) in Area D1

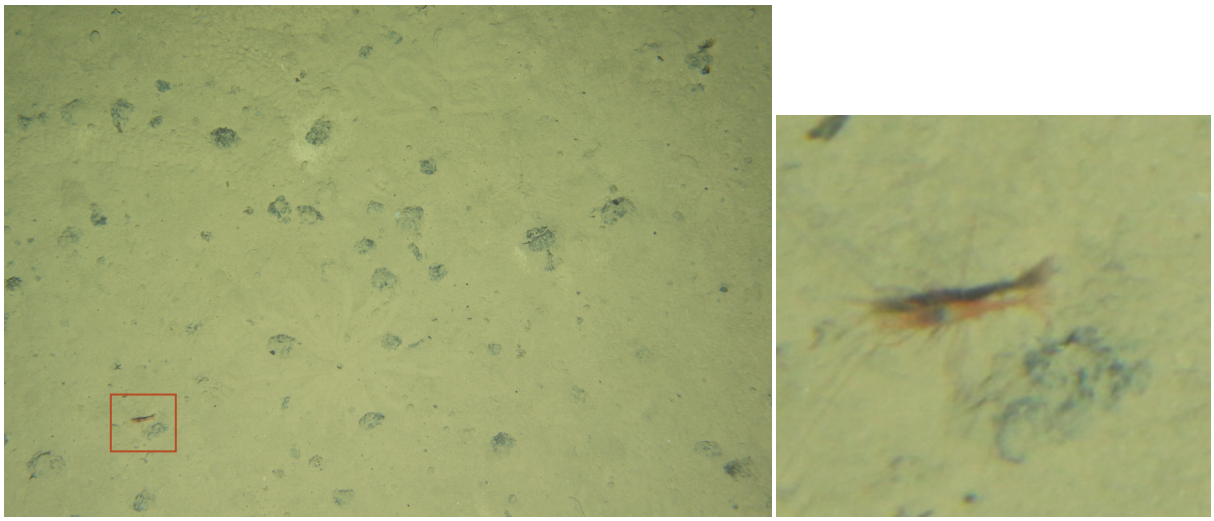

Main photo: 2.4 x 1.5 m; CCZ15-F09B: 2015_09_14_195043

Figure 9.65 Phylum mollusca (bivalve example) in Area B1

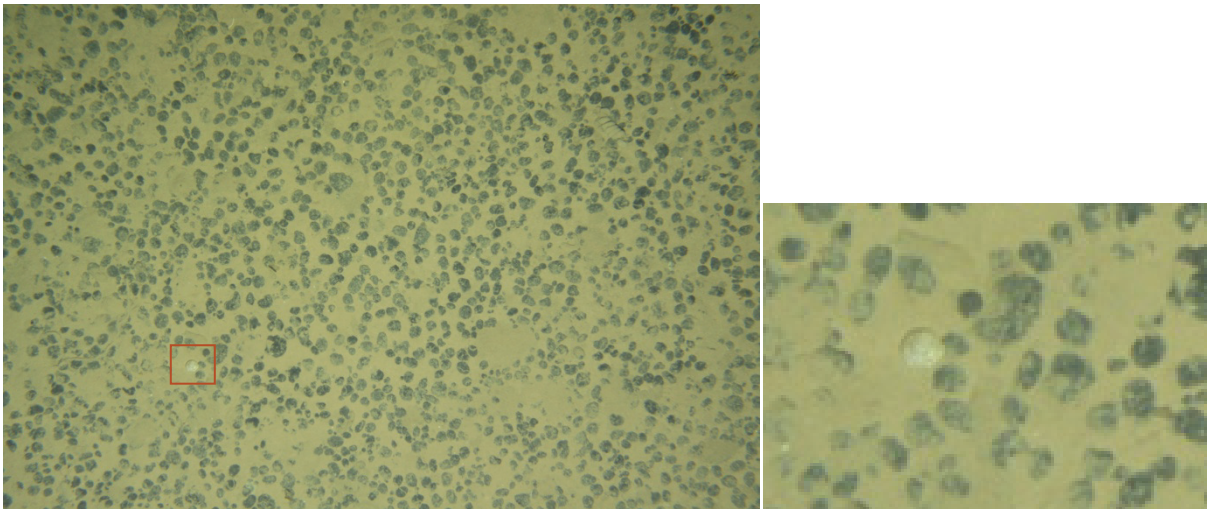

Main photo: 2.4 x 1.5 m; CCZ15-F02: 2015_08_16_195404

Figure 9.66 Class xenophyophorida (protozoan)

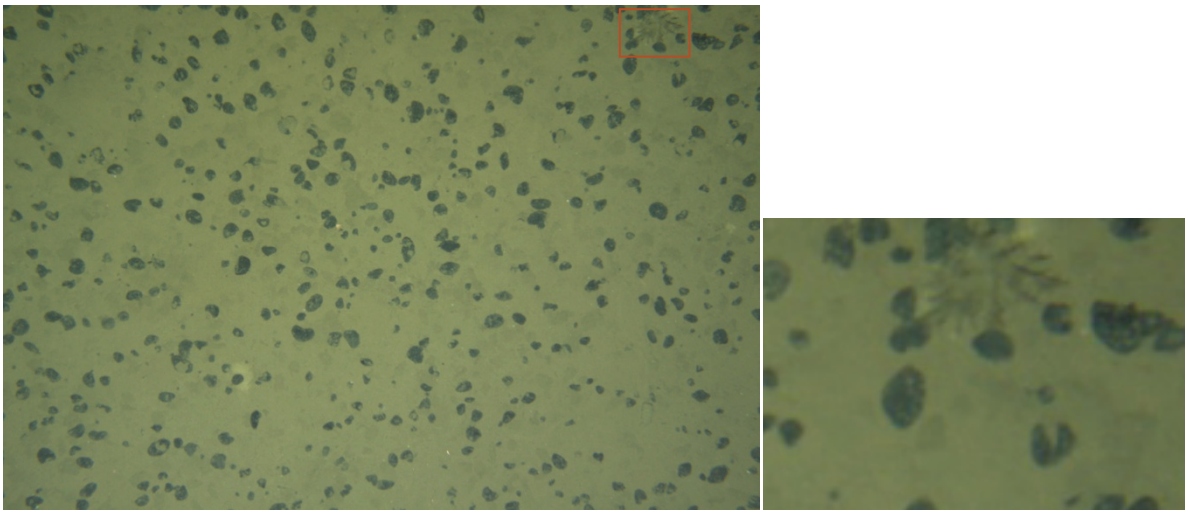

Main photo: 2.4 x 1.5 m; CCZ15-F07: 2015_09_03_190541

9.4.4 TOML Photo-profile based habitat mapping trial

A habitat classification scheme was developed during the CCZ15 cruise that was based on previous work in the CCZ and that adopted elements of existing classifications schemes, namely the US Coastal and Marine Ecological Classification Standard (CMECS, FGDC, 2012), the European Nature Information System (EUNIS, Davies et al. 2004) and the Collaborative and Automated Tools for Analysis of Marine Imagery (CATAMI, Althaus et al. 2015). The TOML scheme contained three components (Geomorphology, Substrate and Biological). The scheme was trialled on TOML area B1 (Figure 9.67, Figure 9.68) with the intent to apply to other areas after review.

Figure 9.67 Areas where biota was not observed

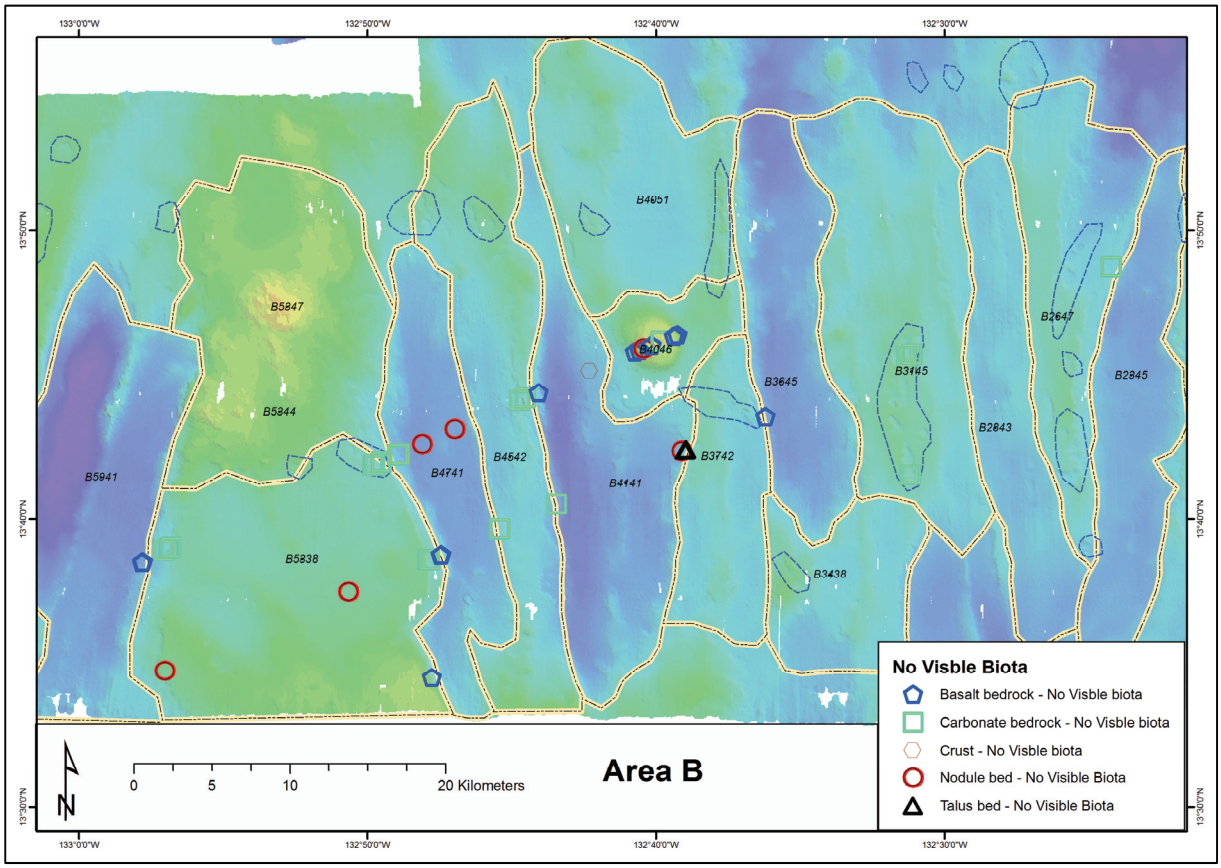

Figure 9.68 Dominant biota observed

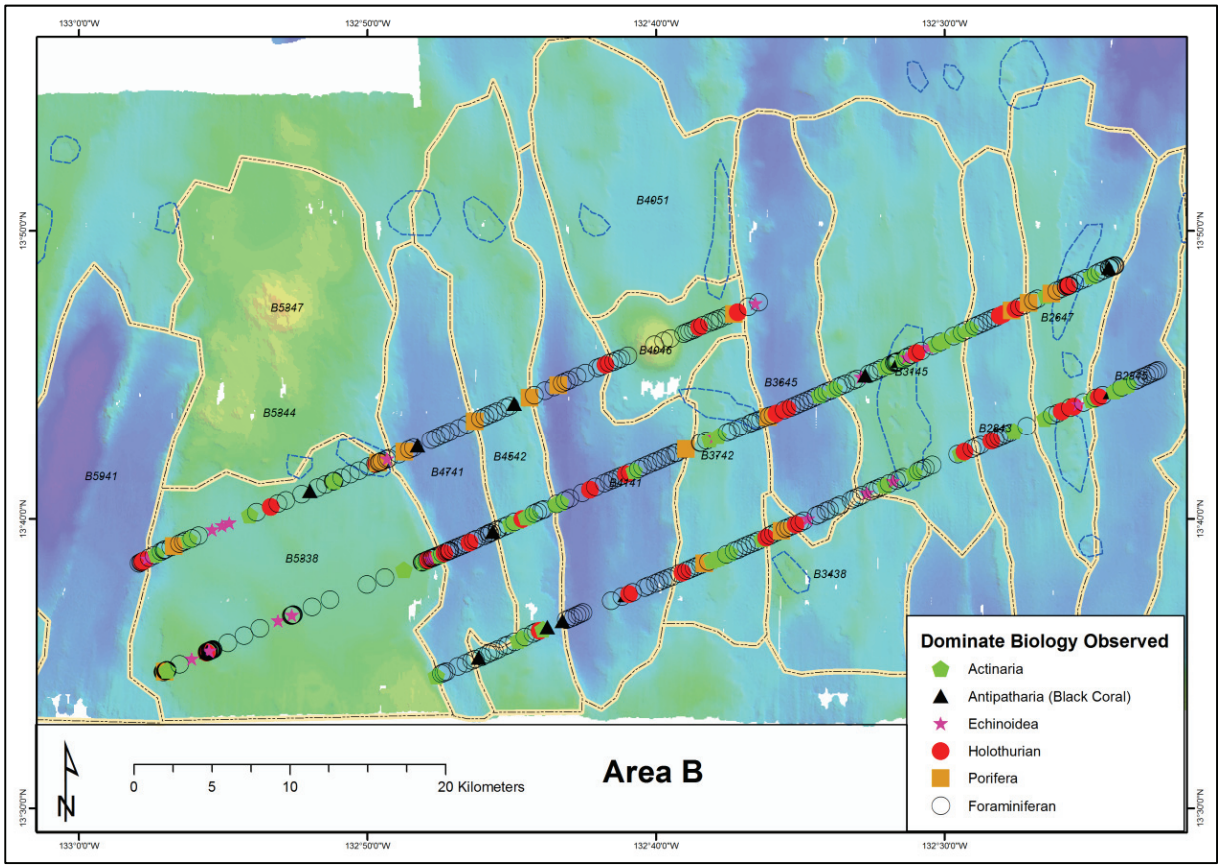

The trial involved detailed classification of every tenth photo taken along three Neptune photo sled lines (CCZ15-F01, F02 and F03). In some areas, the number of photos logged was increased to capture seafloor features that were smaller in area.

Data were analysed to determine if there were any significant relationships between the distribution of benthic biota and the geoforms and substrate types on which they occurred. The analysis made use of boosted regression trees (BRT) via the R statistical software package (R Core Team, 2016) and multivariate cluster analysis via Primer-e software (Clarke and Gorley, 2006). The trial dataset used in the analysis was relatively small and analysis was restricted to fauna that were most abundant in photo logging. Therefore, some caution is needed when interpreting the results. BRT analysis was not extended to investigate variable interactions or predictions of habitat suitability.

9.4.4.1 BRT Results

Actinarians (sea anemones) were predominantly observed in nodule bearing sediment. The BRT results indicated that actinarians were most frequently associated with nodule cover class of 21-40%, 41-60% and >60%. They were most commonly associated with large Type C nodules.

Megafauna-sized foraminifera were observed in the majority of photographs logged. Volcanic and carbonate bedrock were the only substrates that did not support foraminifera.

BRT analysis using a logging class “no visible biota” indicated that the seamount in Area B and step/ledge geoforms were devoid of megafauna. The substrate observed in these areas was volcanic and carbonate bedrock and crust.

9.4.4.2 Cluster Analysis Results

Morphospecies abundance was compiled for each photo frame, along with the four-level Geomorphology and Substrate components logged from each frame. Data from two photo sled lines in Area B were used in this preliminary analysis. The abundance data were transformed to presence-absence. This is the most aggressive form of transformation and so patterns detected using presence-absence data are considered to represent the strongest ecological patterns of interest to the preliminary analysis.

There was no clustering of samples according to Geoform levels 1 and 2. Samples did cluster according to Geoform Level 3 (Figure 9.69), with nodule-bearing sediment forming a somewhat dispersed cluster that overlaps with, but is distinct from, nodule-free sediments. A stress of 0.14 in the multidimensional scaling plot indicates that patterns are fairly well represented in two dimensions. A 3D plot of the same data decreased the stress to 0.1, indicating that there is an important third dimension to the data. Analysis of Similarity (ANOSIM routine) indicated that the difference between nodule-free and nodule-bearing sediments was statistically significant (Global R = 0.326, R significance < 0.05 for pairwise comparison). Rock pavement appeared to form a third intermediate and dispersed group and ANOSIM indicated that the rock pavement samples were significantly distinct from nodule-free sediments and nodule-bearing sediments.

Figure 9.69 Samples (image frames) coded by Geoform Level 3 (L) and 4 (R)

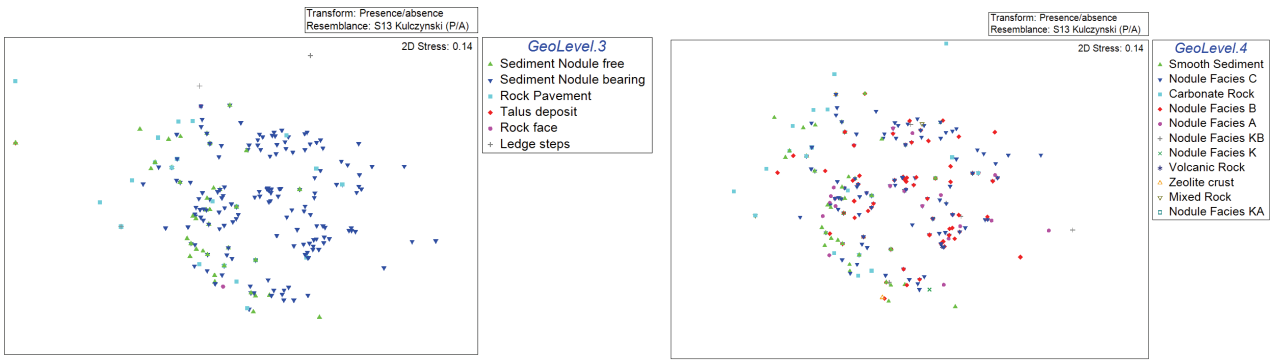

At Geoform Level 4, samples from smooth sediment formed a dispersed but separate cluster from those on nodule-associated geoforms (Figure 9.69) but there was no significant clustering according to nodule facies type, a result confirmed by ANOSIM.

At the Substrate Group level (level 3 of the substrate classification hierarchy) there was dispersion among samples, but samples from nodule-mud mixes and gravels formed a group that was differentiated from mud and mud-nodule mixes (Figure 9.70). These groups represented varying dominance of nodules and ANOSIM indicated that the pairwise difference between nodule-mud mixes and mud-nodule mixes was significant. At level 4 of the substrate classification, nodule density was estimated. Again there was dispersion among samples, but those from high density (41-60%) and very high density (60+%) nodule density substrates clustered separately from the low (6-20%) and very low (1-5%) nodule density substrates (Figure 9.70). ANOSIM indicated that these groups were significantly different. Differences in community composition among substrate types may be expected because nodules represent attachment surfaces for sessile invertebrates that favour hard substrates.

Figure 9.70 Samples (image frames) coded by Substrate Group

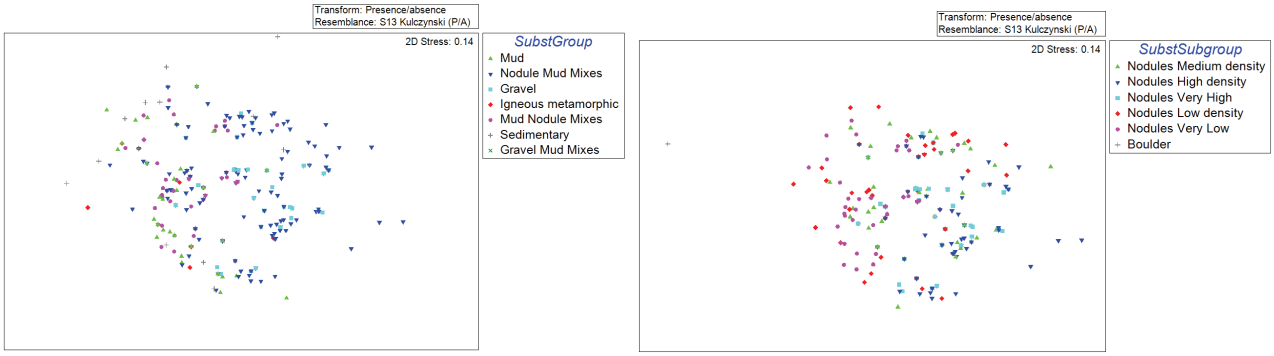

Samples (image frames) coded by Substrate Group (level 3 of the substrate classification at L and level 4 at R)

9.4.4.3 Conclusions of Preliminary Habitat Mapping

The hierarchical physical and biological classification scheme used to log images appears to be suitably sensitive to detect gradients in megafauna community composition and relate these to physical habitat structure. Importantly, preliminary analysis indicated that high-level taxonomic identifications made using the formal scientific classification (e.g. Phylum-level, which are often the only identifications possible from imagery) did not provide suitable resolution to detect differences. The concept of morphospecies identification has been adopted for megafauna in several contemporary marine studies and has been used in the CCZ for nodule-attached foraminifera, where formal taxonomic descriptions are not available (Kamenskaya et al, 2012; Veillette et al, 2007; Gooday et al, 2015).

Specific conclusions of the preliminary analysis are:

- Megafauna communities associated with nodule-free sediments differ from those associated with nodule-bearing sediments.
- Among the nodule-associated group, nodule facies (level 3 Geoform) as they were logged, was not a significant factor in structuring community composition. However, nodule density was significant.
- Based on the preliminary cluster analysis of Area B, a working hypothesis is supported for the existence of four benthic habitat types with respect to megafauna:
  - Sediment: nodule-free: smooth mud.
  - Sediment: nodule-bearing: high to very high density nodule-mud mixes.
  - Sediment: nodule-bearing: low to very low density nodule-mud mixes.
  - Rock pavement: sedimentary carbonate.

Populating Boosted Regression Tree models with additional data is expected to provide additional resolution on fauna distributions and provide a method for predictive habitat suitability modelling and thus support future impact assessment and spatial management of mining.

It is noted that the habitat mapping trial was done across a fairly restricted range of abyssal hill types (Physiographic Setting Subcomponent to Geoform Level 1 in Table 7-3) without any clear discrimination in biology between these types. This needs still to be reconciled with biological differences noted by Melnik and Lygina (2010) at Geoform Level 1 (their Striped, Undulated and Cloak type abyssal hills).

9.4.5 Other results

9.4.5.1 Dredging

Seventeen sites have been sampled either by epibenthic sled (CCZ13 cruise; Figure 9.31) or Galatea dredge (CCZ15 cruise; Figure 9.32).

Figure 9.71 Dredge sample locations CCZ13 and CCZ15

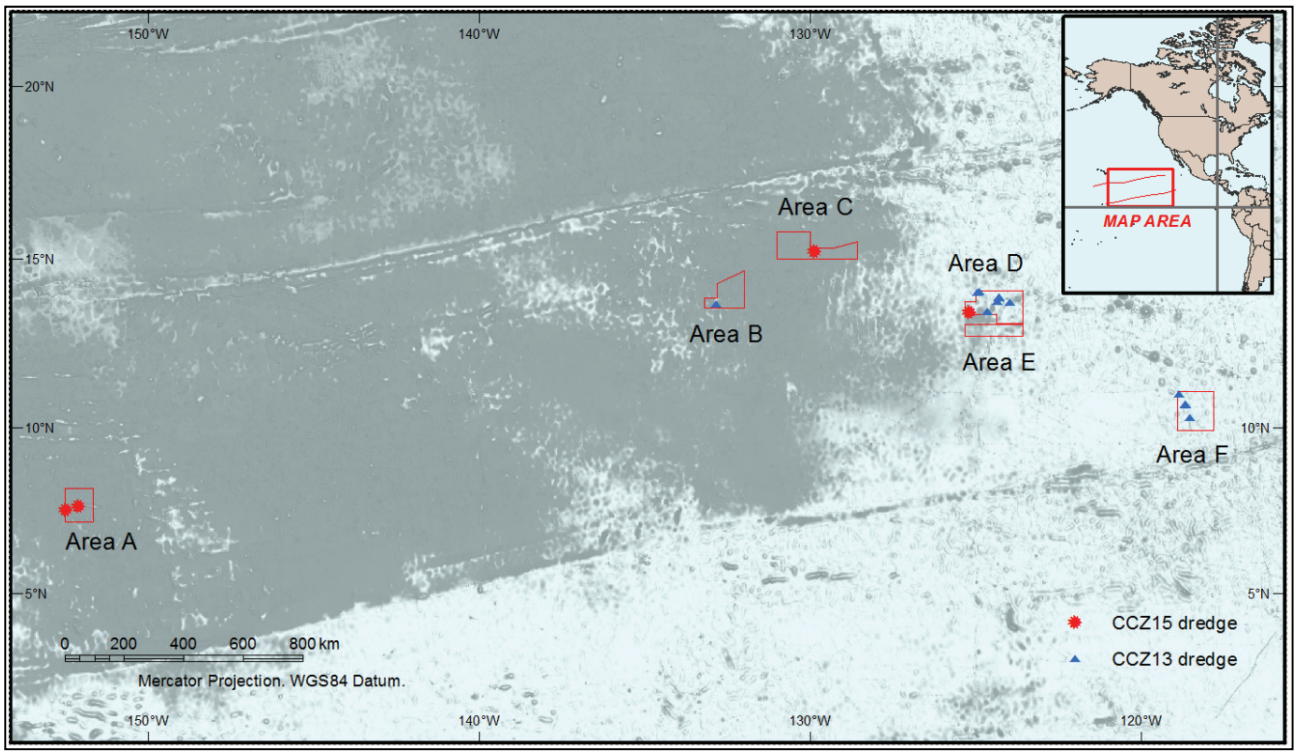

The samples were logged and:

- Sub-sampled extensively (up to 30 fragments per dredge sample) to confirm historical grades and to study variability in grade (which was shown to be extremely low (Item 12);
- Used in drying testwork already reported in section 7.6;
- Used for metallurgical test work.

9.4.5.2 Towed Sonar - Side Scan

Sidescan sonar was used to map/characterise parts of several of the sub-areas for which an Indicated Mineral Resource is defined in Item 14. In effect these sub-areas are future options for TOML to conduct pilot, trial, and early commercial mining operations and are called Priority Mining Areas (PMA) in ISA terminology. An example of survey over the B5338 field within the B1 sub-area, is presented here.

In B5338 and the other areas, features of note on the side-scan and sub-bottom profiler can be classified into five categories:

- Texture relating to nodule coverage/size (and thus nodule abundance)
- Mapping of obstacles of concern in any future mining operation
- Detailed bathymetry (slopes and orientations of slopes)
- Textures and profiles relating to sediment types
- Features that imply a particular geological history.

Nodule coverage in B5338 is consistent on the top of the ridge with a clear correlation with photo-profile coverage (Figure 9.53).

The most significant obstacles are the slopes defining the eastern and western boundaries of B5338, but there are also areas within the sub-area that could likely hinder a mining system. These include incipient karstic features and a basalt outcrop. There is also one steep small ridge as well as a small basalt floored karstic feature in the SW. Apart from these, however, the surface looks very smooth even with local ridge systems of several tens of metres altitude.

The sub-bottom profile data (not shown) show good development of a typical CCZ stratigraphy (Item 7) with thinning of siliceous ooze to the north.

In the northern area peculiar dome-shaped features (~1 km diameter) are visible on the side-scan (Figure 9.72). These appear to be the result of block faulting. Sub-surface carbonate dissolution is indicated in the sub-bottom profiler at depth both in B5338 and in adjacent valley B4741 but these do not express at surface.

Figure 9.72 Side scan coverage and geological interpretation of the B5338 field, Area B1

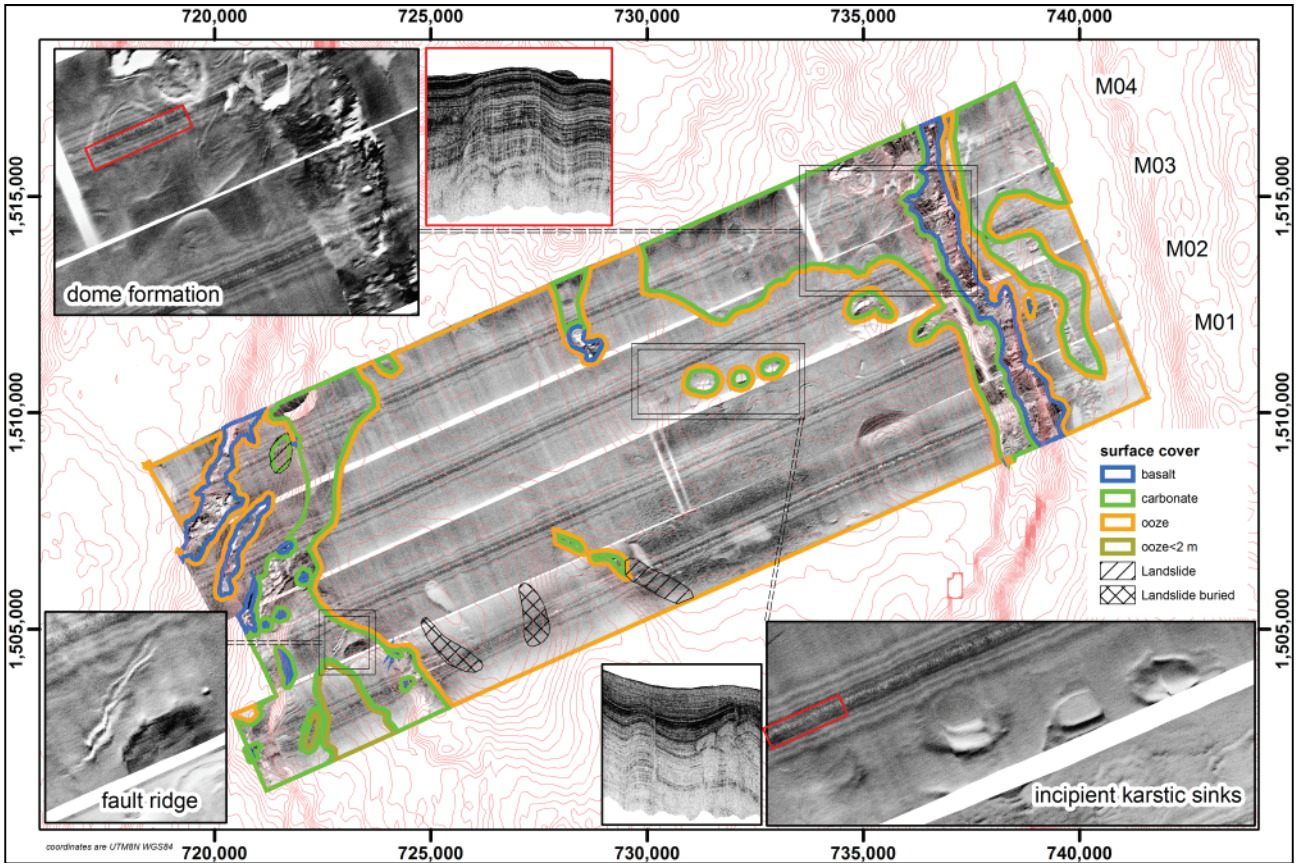

Swath is ~ 2km wide and sub-bottom profile thickness is ~ 100 m at V/H=10:1

9.4.5.3 Towed Sonar – Sub-bottom Profiler

The sub-bottom profiler was used to classify types of abyssal hills. Figure 9.73 shows profiles with three types of abyssal hill:

- GH stands for graben-horst and is the most rugged topography with fully developed grabens (valleys) and intermediate horsts (hills)
- UH stands for undulating hills and is less rugged than GH and typically includes half-grabens and warped rather than fault-blocked topography
- GU stands for gently undulating and is the most, gentle land form with warped gently undulating topography.

These types of abyssal hills inform the physiographic scale geomorphology units described in Table 7.4.

Figure 9.73 Abyssal hill classification from sub-bottom profiles

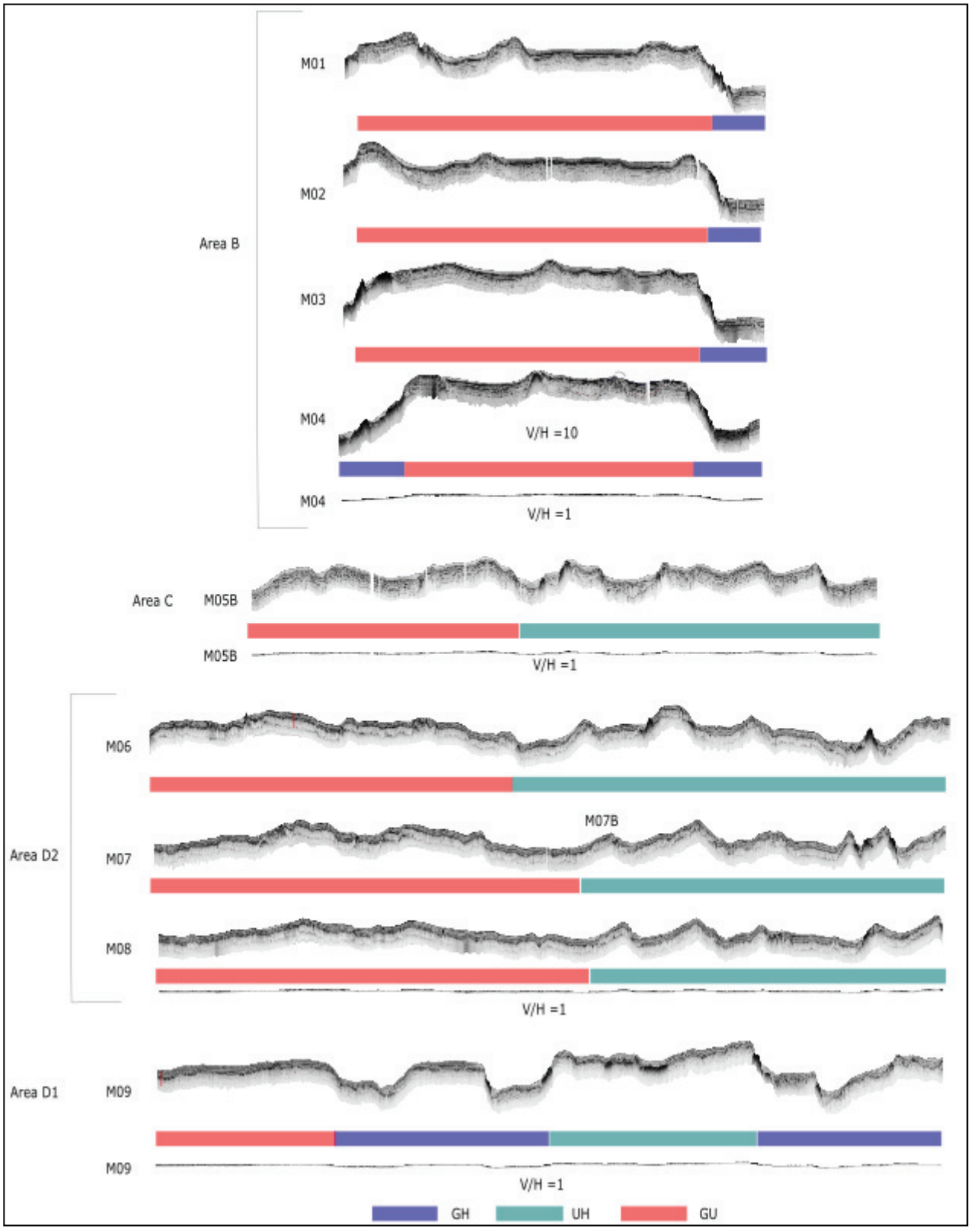

A range of other geological features can been seen on the sub-bottom profile sections, including faults, collapse features (probably related to a combination of faulting and carbonate dissolution; (Figure 9.74) and recent igneous activity including dykes (Figure 9.75) and sills (Figure 9.76). Of note are the “basin type” dissolution horizons that are found almost exclusively in grabens or down-warped areas. They have distinctly different sonar signature to the karstic features that typically form on hill crests.

Figure 9.74 Fault bound collapse-dissolution in carbonate

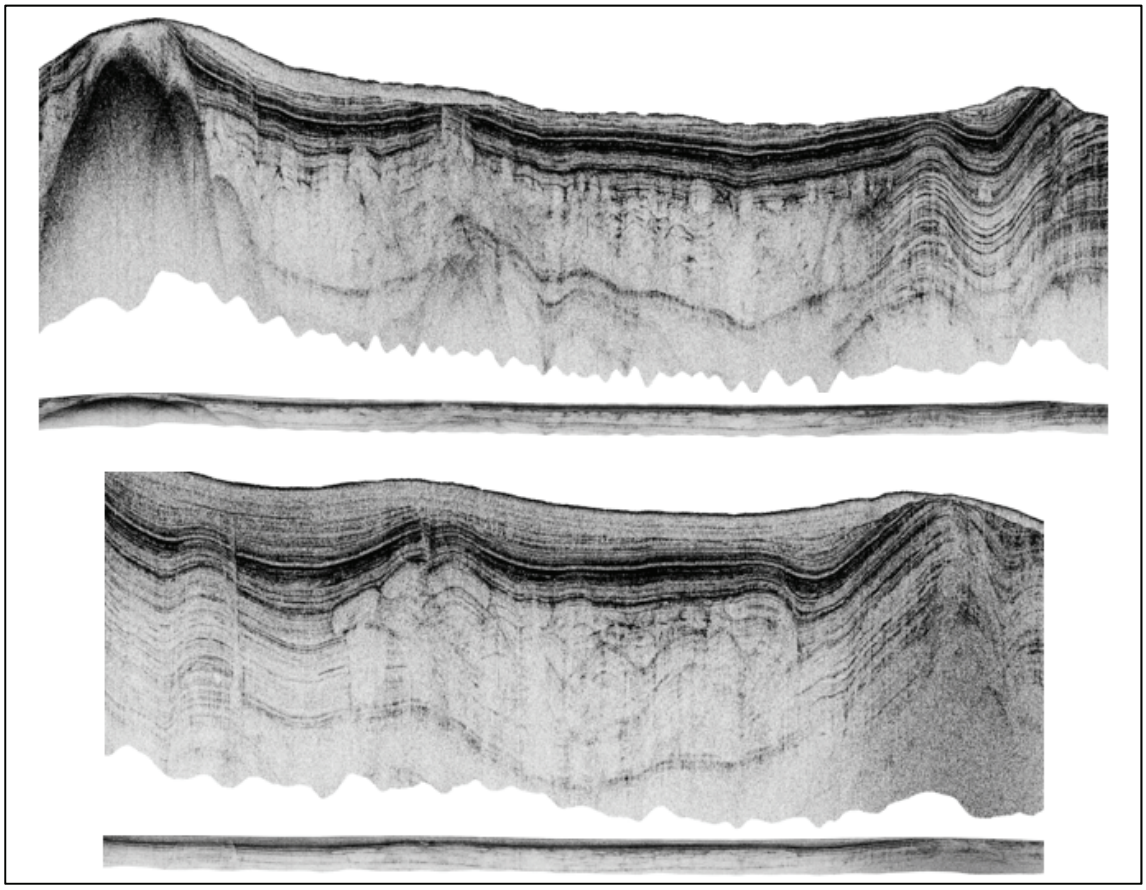

Profile is about 100 m thick: CCZ15-M04_(T), CCZ15-M03_(B) each section pair is V/H=10, and V/H=1

Figure 9.75 Possible dyke swarm in western subarea D 3454

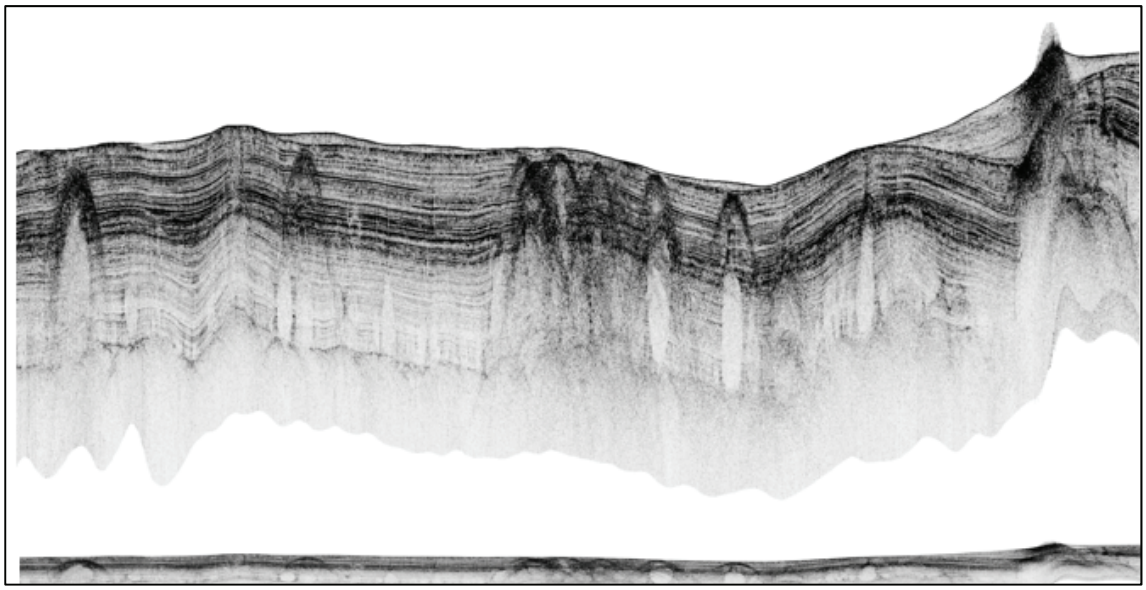

Profile is about 100 m thick: (CCZ15-M06) section pair is V/H=10, and V/H=1

Figure 9.76 Possible late stage sill or peperite layer and feeders in DW0332, Area D1

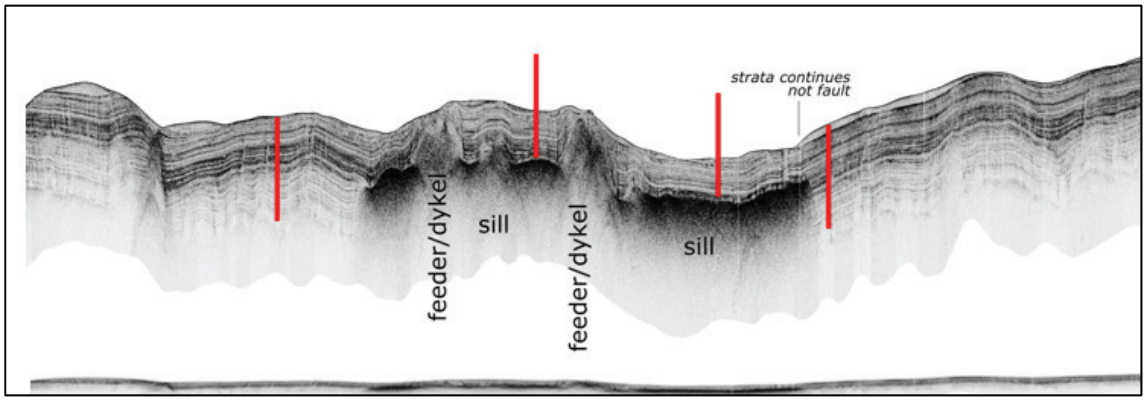

Profile is about 100 m thick: section pair is V/H=10, and V/H=1

9.4.5.4 Relationship with backscatter

An indirect relationship between nodule abundance and acoustic response has been known for many years (e.g. ISA, 2010; Ruhlemann et al, 2011), and this was confirmed by the results of the two TOML cruises. Essentially the backscatter response (or reflection) can be used in many cases to discriminate:

- Rock from sediment
- Sediment types (e.g. Calcareous versus siliceous)
- Sediment with or without nodules
- Sediment with larger or smaller nodules (and larger nodules often result in higher abundance).

An example of characterisation is illustrated in Figure 9.77 and this response played a role in the map shown in Figure 9.72. The continuous nature of the nodules is evident from both acoustics and photo logging. Figure 9.78 quantifies the fair correspondence between abundance and acoustic reflectance and abundance and nodule coverage for TOML area B1.

Figure 9.77 Characterised MBES backscatter response in B5338

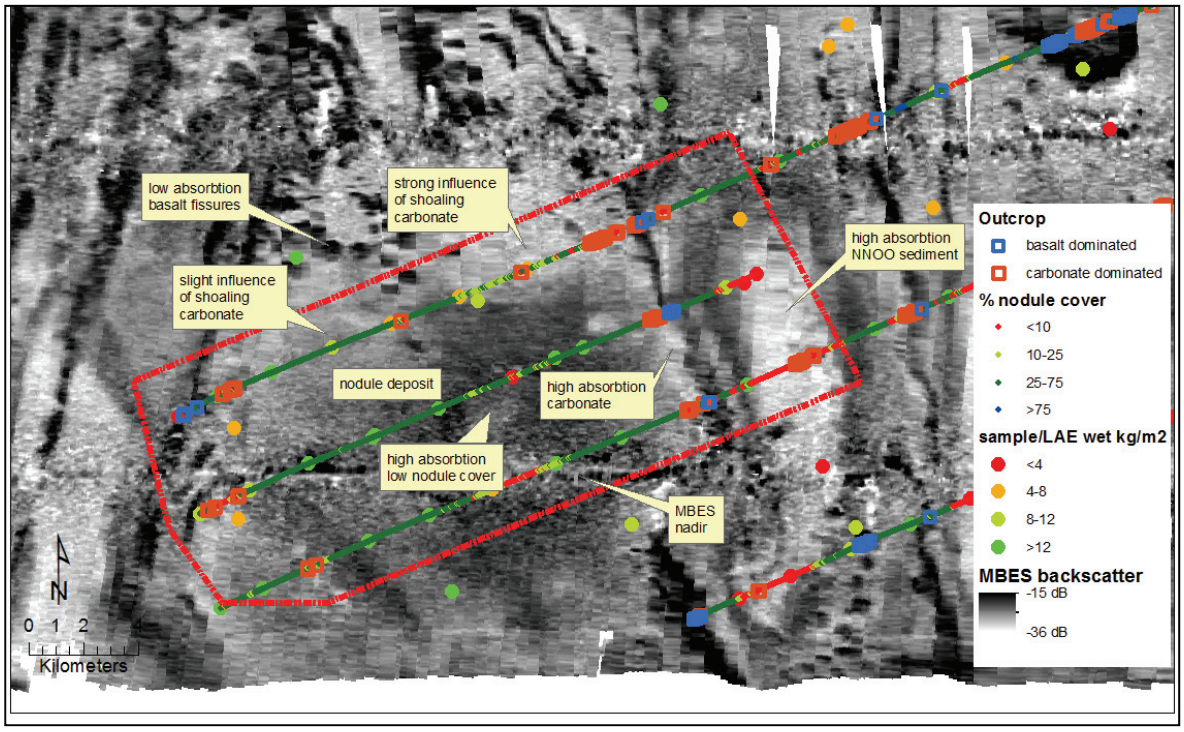

Nodule cover from photo-profile lines ~3.5 km apart.

Figure 9.78 Relationships between abundance and acoustic reflection and nodule coverage

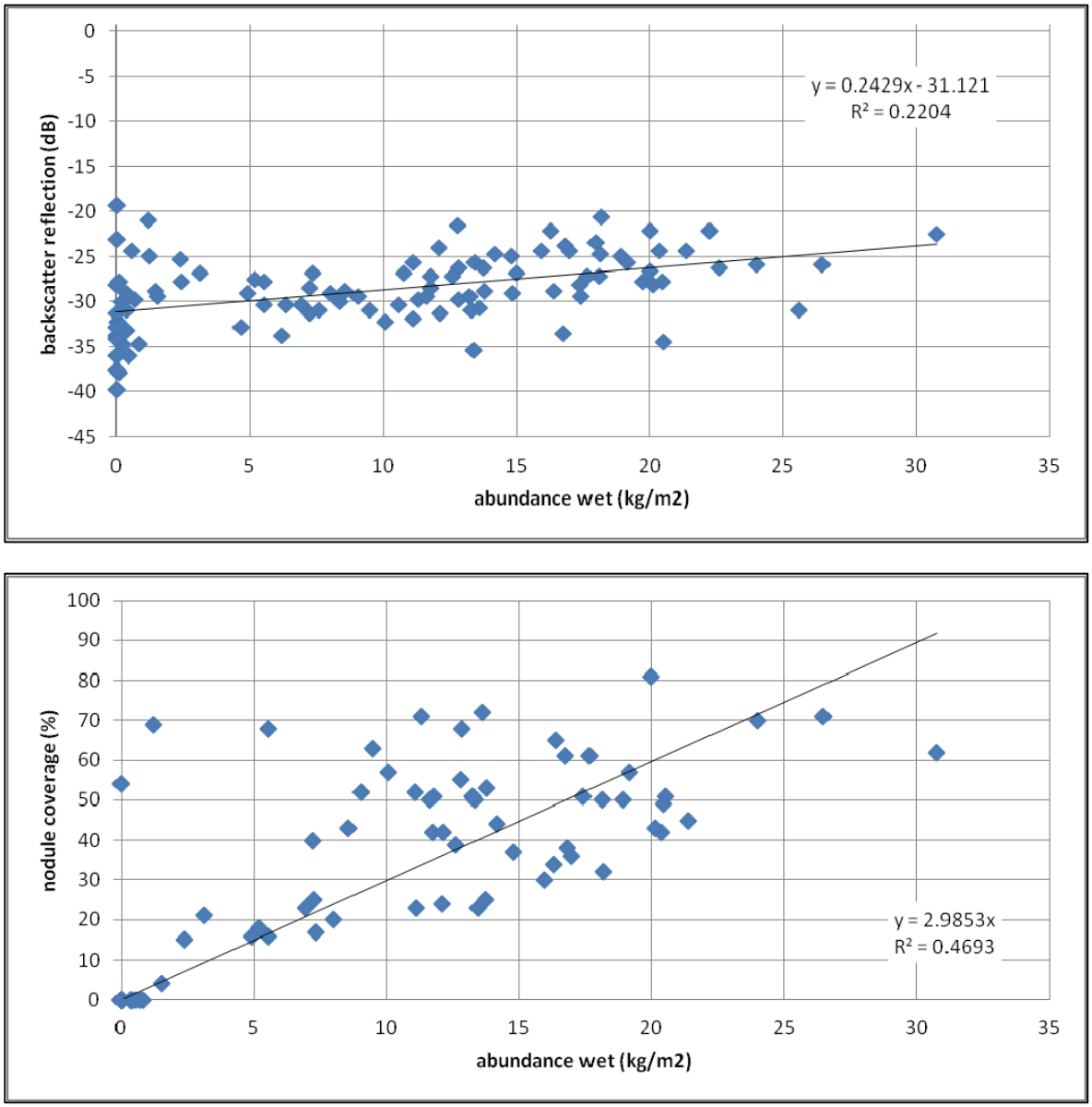

Area B1, include long-axis based estimates of nodule abundance